Collisional-Radiative Model of Quasi-Stationary Helium Plasma and Its Application to the Plasma in Positive Column

AUTHOR(S):

OGATA, Yoshiro; FUKUDA, Kuniya

Collisional-Radiative Model of Quasi-Stationary Helium Plasma and Its Application to the Plasma in Positive Column

By

Yoshiro OGATA* and Kuniya FUKUDA**

(Received December 28, 1972)

Abstract

The collisional-radiative model is applied to a quasi-stationary helium plasma and the collisional-radiative and population coefficients are calculated, provided that the level system of helium atom is composed of the ground level 1^1S, the four lowest excited levels, 2^3S, 2^1S, 2^3P and 2^1P, and higher hydrogenic levels. The ranges of plasma parameters are $8\times10^3 \leqq T_e \leqq 1.28\times10^5$ °K and $10^5 \leqq n_e \leqq 10^9$ cm^{-3}, and the results are compared with the data by Drawin *et al.*

Next, the model is applied to a positive-column helium plasma and the plasma balance equation in the case of ambipolar diffusion is simultaneously solved with a set of rate equations for excited helium levels which includes the diffusion of atoms in metastable states. The results give the relation among the filling gas pressure in a discharge tube, plasma parameters and population densities of the excited levels. The atomic processes of ionization, excitation and deexcitation in the plasma are analyzed in detail.

1. Introduction

Recently atomic processes in a positive-column plasma have been extensively studied and it has been reported that helium atoms in metastable states play an important role in the ionization of the plasma. For example, in a metal laser plasma, Penning ionizing collisions with metastable helium atoms are essential to create metal ions in the laser upper level[1-3] and in pure helium plasma the stepwise ionization through the four lowest excited levels[4,5] or through higher excited levels[6,7] makes an important contribution to determine the plasma condition. In the present paper the calculations, which combine the plasma balance equation with the collisional-radiative model of plasma,[8,9] are made to examine the contributions from helium atoms in low-lying excited levels, 2^3S, 2^1S, 2^3P and 2^1P, to the ionization of a positive-column plasma and also to make clear the atomic pro-

* Department of Mechanical Engineering II. Present address: Research Laboratory, Matsushita Electronics Corporation

** Department of Mechanical Engineering II

cesses controlling these levels in the practical ranges of plasma parameters.

The calculation of population densities based on the collisional-radiative model was made by the present authors on the optically thin hydrogen plasma in a positive-column.[10] However, in this calculation the plasma parameters were taken arbitrarily so that the results are not applicable to an actual plasma. Drawin *et al.* calculated the collisional-radiative ionization and recombination coefficients[11] as well as the population coefficients[12] for a quasi-stationary helium plasma and the results were applied to the helium plasma in a stationary PIG-discharge.[13]

The present calculation of the coefficients in the collisional-radiative model of a quasi-stationary helium plasma is quite similar to that by Drawin *et al.* However, the rate coefficients for the radiative and collisional transitions between low-lying excited levels are newly derived from the most probable data of cross sections and those concerned with high-lying excited levels are calculated to give a consistency with the assumed energy level system of helium atom. The calculated values of the collisional-radiative and population coefficients are tabulated in section 2 and compared with the data of Drawin *et al.*

In section 3 the plasma balance equation is combined with the collisional-radiative model to make clear the atomic processes in a positive-column helium plasma. The equation consists of a balance between the ion diffusion to wall and ion production from plasma. The free-fall[14] or ambipolar diffusion[15-17] theory is used depending on the discharge conditions, *i.e.*, the filling gas pressure and bore radius of a discharge tube. The present calculation is made for the discharge conditions which allow the latter theory. Further, the diffusion of metastable helium atoms is taken into account in the rate equations of the collisional-radiative model. The calculation is carried out in the practical ranges of plasma parameters. The results given in section 4 enable us to examine quantitatively the ionization, excitation and deexcitation processes of excited helium atoms in a positive-column helium plasma.

2. Collisional-Radiative Model of Quasi-Stationary Helium Plasma

The collisional-radiative model[8,9] is applied to a quasi-stationary helium plasma, and the collisional-radiative ionization and recombination coefficients as well as the population coefficients are calculated. The procedure is described in detail in refs. 10 and 18.

The rate of variation of the population density $n(i)$ of a level i is given by

$$\dot{n}(i) \equiv \frac{\mathrm{d}n(i)}{\mathrm{d}t} = n_e \sum_{j=1}^{i-1} n(j)\, C(j,i)$$
$$- n(i)\left[n_e\left\{\sum_{j=i+1}^{\infty} C(i,j) + \sum_{j=1}^{i-1} F(i,j) + S(i)\right\} + \sum_{j=1}^{i-1} A(i,j)\right]$$
$$+ \sum_{j=i+1}^{\infty} n(j)\left\{n_e F(i,j) + A(i,j)\right\} + n_i n_e\left\{n_e \alpha(i) + \beta(i)\right\}, \qquad (1)$$

where n_e and n_i are the number densities of electrons and ions, respectively, $C(i,j)$ is the rate coefficient for collisional excitation from i to j level by electrons, $F(j,i)$ is that for collisional deexcitation from j to i level, $S(i)$ is that for collisional ionization from the level i, $\alpha(i)$ is that for three-body recombination, $\beta(i)$ is that for radiative recombination and $A(i,j)$ is the Einstein coefficient for spontaneous emission from i to j level.

In the collisional-radiative model $n(i)$ is represented by

$$n(i) = Z(i) n_i n_e r_0(i) + \frac{Z(i)}{Z(1)} r_1(i)\, n(1), \qquad i=2, 3, \cdots, \qquad (2)$$

where $r_0(i)$ and $r_1(i)$ are the population coefficients and $Z(i)$ represents the modified Saha relation;

$$Z(i) = \frac{n_E(i)}{n_i n_e} = \frac{g(i)}{2\omega_i}\left(\frac{h^2}{2\pi m k T_e}\right)^{3/2} \exp\left(\frac{\chi(i)}{kT_e}\right). \qquad (3)$$

Here $n_E(i)$ is the population density of level i in LTE, $g(i)$ and $\chi(i)$ are the statistical weight and ionization potential of the level i, respectively, ω_i is the partition function of the ion, T_e is the electron temperature, m is the electron mass, h is Plank's constant and k is Boltzmann's constant. The population density of the ground level $n(1)$ of Eq. (2) is expressed by

$$\frac{\mathrm{d}n(1)}{\mathrm{d}t} = -n_e n(1) S_{\mathrm{C\text{-}R}} + n_e n_i \alpha_{\mathrm{C\text{-}R}}, \qquad (4)$$

where $S_{\mathrm{C\text{-}R}}$ and $\alpha_{\mathrm{C\text{-}R}}$ are the collisional-radiative ionization and recombination coefficients, respectively.

In the present calculation the system of energy levels of helium atom is assumed to be given in Table 1. The system is composed of the ground level, 1^1S, the four lowest excited levels including two metastable states, 2^3S, 2^1S, 2^3P and 2^1P, and higher hydrogenic levels. The last ones have the statistical weight $4q^2$, where q is the principal quantum number, and the energy values of these levels are approximated to χ_H/q^2, where χ_H is the ionization potential of atomic hydrogen. As shown in Table 1, all the levels are numbered with i instead of q in the order of decreasing ionization potential $\chi(i)$ from the ground level. The effective quan-

Table 1. Energy level system of atomic helium.

level number	principal quantum number	terms included	ionization potential	effective principal quantum number	statistical weight
i	q		$\chi(i)$ (°K)	q'	$g(i)$
1	1	1^1S	285000	1	1
2	2	2^3S	55300	2.27	3
3	2	2^1S	46100	2.49	1
4	2	2^3P	42000	2.60	9
5	2	2^1P	39100	2.70	3
i	$i-3$	all terms with $q=i-3$	χ_H/q^2	q	$4q^2$
.	.	.	.	.	.
.	.	.	.	.	.
.	.	.	.	.	.

$\chi_H = 158000$ °K : Ionization potential of atomic hydrogen

tum number q' is defined as $q'=\sqrt{\{\chi(1)/\chi(i)\}}$ for the four lowest excited levels $i=2$ to 5. The level number i is used for all helium levels in the present paper.

The coefficients $A(i, 1)$ are, of course, zero for the transitions from the metastable states $i=2$ and 3. The coefficients $A(4, 3)$ and $A(5, 2)$ of the intercombination transitions are also zero. The values of $A(5, 1)$, $A(4, 2)$ and $A(5, 3)$ are given in NBS table.[19] The coefficients $A(i,j)$ for $i=6\sim15$ and $j=1$ are calculated from the weighted mean of A-coefficients of helium levels[19] included in the level i with respect to their statistical weights. For the transitions from the levels $i=6\sim13$ to the levels $j=2\sim5$ $A(i,j)$ are calculated in the same way. Yet, for the transitions from the levels $i\geq14$, the lower levels $j=2\sim5$ are assumed to be a single hydrogenic level with $q=2$ and the hydrogen coefficient $A(i, q=2)$ derived from the approximate formula[20] is divided into $A(i,j)$ for each lower level with its statistical weight. For the transitions between hydrogenic levels $A(i,j)$ is, of course, calculated from the approximate formula of the atomic hydrogen.[20] All the values of $A(i,j)$ are listed in Table 2. Further, the values of corresponding absorption oscillator strengths $f(i,j)$ are listed in Table 3.

Cross sections for the electronic collision excitation are determined as follows. $1^1S\rightarrow2^3S$: Drawin's semiempirical formula[21] (DF) is multiplied by 3 by reference

to the calculation by Ochkur *et al.*[22] and the measurement by Zapesochnyi.[23]

$1^1S \rightarrow 2^1S$: DF is multiplied by 2.5 by reference to the calculations by Vriens *et al.*[24] and by Bell *et al.*[25] and the measurement by Zapesochnyi.[23]

$1^1S \rightarrow 2^3P$: DF is multiplied by 2.1 by reference to the calculation by Burke *et al.*[26] and the measurement by Jobe *et al.*[27]

$1^1S \rightarrow 2^1P$: DF is employed by reference to the calculations by Burke *et al.*[26] and by Ochkur *et al.*[28] and the measurements by van Eck *et al.*[29] and by Vriens *et al.*[30]

$2^3S \rightarrow 2^1S$: Drawin[21]

$2^3S \rightarrow 2^3P$: DF is multiplied by 2 by reference to the calculations by Burke *et al.*[26] and by Moiseiwitsch.[31]

$2^3S \rightarrow 2^1P$: A constant value 1.8×10^{-16} cm^2 is employed by reference to the calculation by Burke *et al.*[26]

$2^1S \rightarrow 2^3P$: Eq. (44) of Drawin[21] is adjusted so that the maximum value of a cross section fits the one of the calculation by Burke *et al.*[26]

$2^1S \rightarrow 2^1P$: Drawin[21]

$2^3P \rightarrow 2^1P$: Drawin[21]

The cross sections determined in this way are shown in Fig. 1. For other transitions, DF is employed. The rate coefficient for collisional deexcitation is obtained from detailed balancing. The cross sections for collisional ionizations are as follows. For the ionization from the ground level DF is employed by ref-

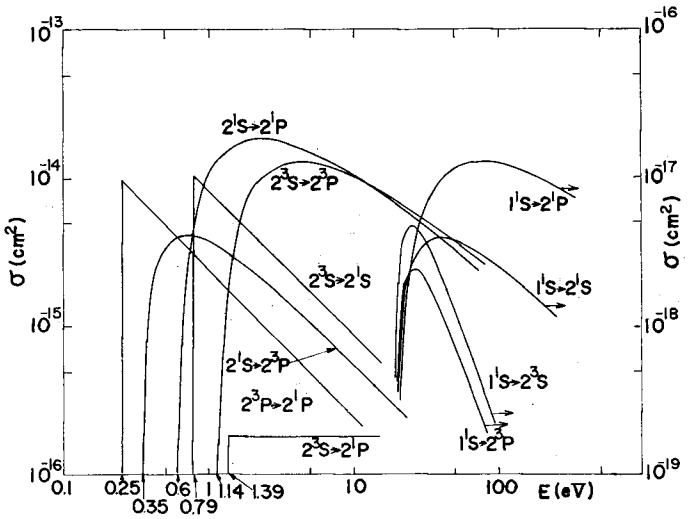

Fig. 1. Cross sections $\sigma(E)$ for electronic collision. The curves for the transitions from the ground level to excited levels are referred to the ordinate in the right side.

erence to the source material.[32-34] For the ionization from the 2^3S level DF is employed by reference to the measurement by Long *et al.*[35] For the ones from other excited levels DF is employed. The rate coefficient for three body recombination is obtained from detailed balancing. The rate coefficient for radiative recombination is given by Drawin *et al.*[12]

The calculation is carried out for both optically thin and thick plasma in the ranges of plasma parameters of $8\times10^3\leq T_e\leq1.28\times10^5$ °K and $10^5\leq n_e\leq10^{19}$ cm^{-3}. In the latter case all $A(i, 1)'$s are assumed to be zero. All levels from the ground level to the level $i=21$ are included in the calculation. It is assumed that the level of the higher limit ($i=21$) is in LTE.

The calculated values of the population coefficients $r_0(i)$ and $r_1(i)$ are given for the optically thin plasma in Tables 4 and 5, respectively. Except for the case of low temperature ($T_e<10^4$ °K), these values agree with the ones calculated by Drawin *et al.*[12] within the factor of ten. Examples of electron density dependences of $r_0(i)$ and $r_1(i)$ are shown in Figs. 2(a) and (b), respectively, for both optically thin and thick plasmas at $T_e=5\times10^4$ °K. The behaviors of the metastable states differ from the ones of other levels as follows; as n_e increases, $r_0(2^3S)$ and $r_0(2^1S)$ decrease lineraly with n_e for $n_e\lesssim10^{12}$ cm^{-3}. The coefficients $r_1(2^3S)$ and $r_1(2^1S)$ have no "coronal" phase and are independent of n_e for $n_e\lesssim10^{11}$ cm^{-3}.

The calculated values of the collisional-radiative coefficients S_{C-R} and α_{C-R} are listed for the optically thin plasma in Tables 6 and 7, respectively. These values agree fairly with the ones calculated by Drawin *et al.*[11] Examples of electron

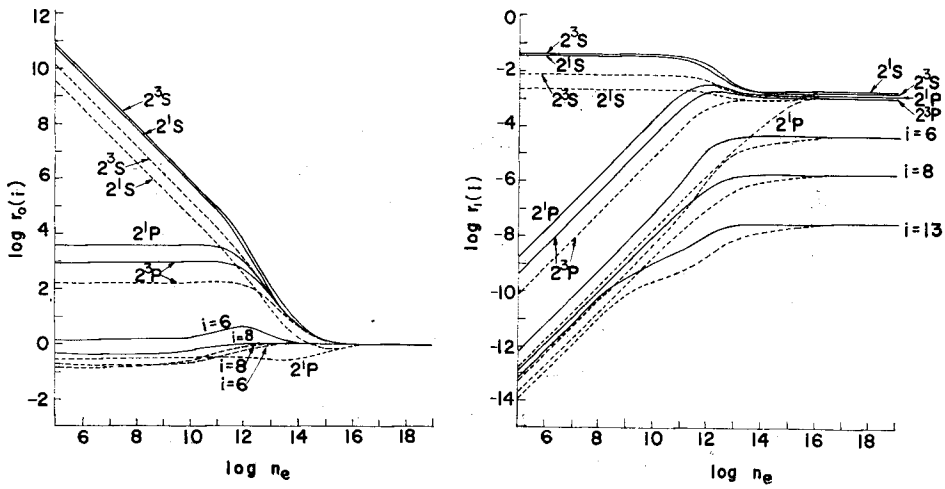

Fig. 2. The population coefficients (a) $r_0(i)$ and (b) $r_1(i)$ versus electron density n_e(cm^{-3}) at $T_e=5\times10^4$ °K. – – –; optically thin. ——; optically thick towards all resonance lines.

density dependences of S_{C-R} and α_{C-R} are shown for both optically thin and thick plasmas at various electron temperatures in Figs. 3 and 4, respectively.

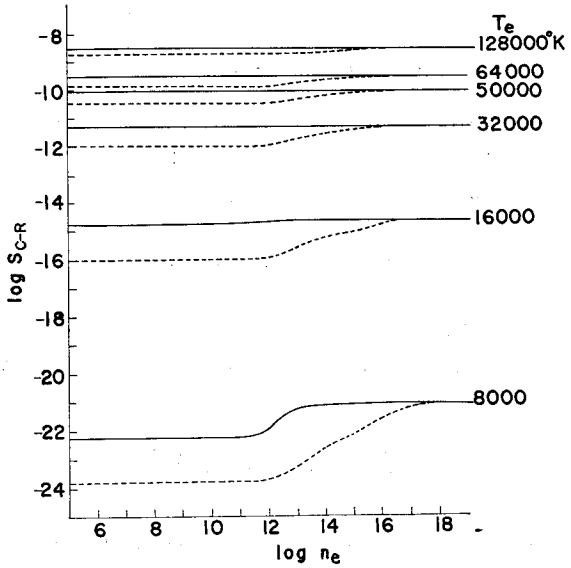

Fig. 3. The collisional-radiative ionization coefficient S_{C-R} (cm^3sec^{-1}) versus electron density n_e(cm^{-3}) for various electron temperatures T_e(°K). – – –; optically thin. ——; optically thick towards all resonance lines.

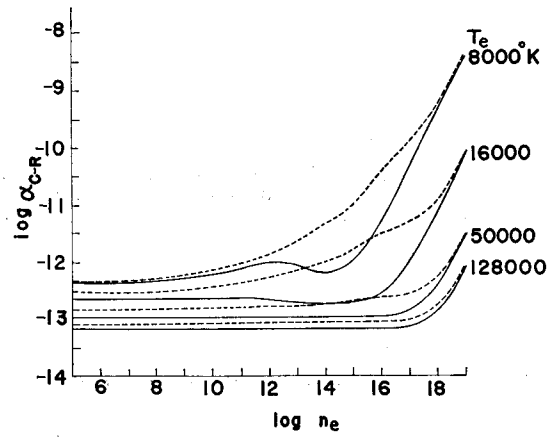

Fig. 4. The collisional-radiative recombination coefficient α_{C-R} (cm^3sec^{-1}) versus electron density n_e(cm^{-3}) for various electron temperatures T_e(°K). – – –; optically thin. ——; optically thick towards all resonance lines.

3. Helium Plasma in a Positive Column

The ambipolar diffusion theory of low ionized plasma in a low pressure cylindrical positive column was formulated by Schottky[15] for the case of a one-stage ionization and the plasma balance equation was given as

$$R\sqrt{Z/D_a} = 2.405\,, \tag{5}$$

where R is the radius of the column, Z is the rate of one-stage ionization by electron collision and D_a is the ambipolar diffusion coefficient.

The ambipolar diffusion coefficient is given as

$$D_a = \frac{kT_e}{e}\frac{760}{p}\mu \quad \mathrm{cm^2\,sec^{-1}}\,, \tag{6}$$

where e is the electronic charge, p is the filling pressure in Torr and μ is the ion mobility at 760 Torr and 300 °K in $\mathrm{cm^2\,V^{-1}\,sec^{-1}}$. Due to sheath effect[5] the ion mobility must be multiplied by

$$1+8.5\left(\frac{\lambda_D(0)}{R}\right)^{2/3}+10.0\left(\frac{\lambda_D(0)}{R}\right)^{4/3}, \tag{7}$$

where $\lambda_D(0)$ is the Debyė shielding length at the axis of the column in cm. The ion mobility has the ion temperature dependence as follows:

$$\mu(T_{\mathrm{ion}}) = \frac{2.7}{1+0.1\times T_{\mathrm{ion}}{}^{1/2}}\mu \tag{8}$$

where T_{ion} is the ion temperature in °K. In combination with Eqs. (6), (7) and (8), Eq. (5) is rewritten as

$$\frac{Z}{r} = 1\,, \tag{9}$$

where

$$r = \left(\frac{2.405}{R}\right)^2\frac{T_e}{11600}\frac{760}{p}\left\{1+8.5\left(\frac{\lambda_D(0)}{R}\right)^{2/3}+10.0\left(\frac{\lambda_D(0)}{R}\right)^{4/3}\right\}$$
$$\times\frac{2.7}{1+0.1\times T_{\mathrm{ion}}{}^{1/2}}\mu\ \mathrm{sec^{-1}}\,. \tag{10}$$

The value of μ used in the calculation is 10.4.[36]

When the stepwise ionizations from all the excited levels are considered, the rate Z is given as

$$Z = \sum_{i=1}^{\infty} n(i)\,S(i) \quad \mathrm{sec^{-1}}\,. \tag{11}$$

For low ionized plasma, $n(1)$ in Eq. (11) is written by

$$n(1) = 3.54 \times 10^{16} p_{\text{gas}}, \tag{12}$$

where p_{gas} is gas pressure in Torr, which is described as

$$p_{\text{gas}} = \frac{273}{T_{\text{gas}}} p \tag{13}$$

at the gas temperature T_{gas} (°K) under discharge.

In a positive-column helium plasma metastable atoms are destroyed by the diffusion to the wall, and so new definitions of A-coefficient,

$$A(2, 1) = \frac{D_2}{\Lambda^2} \tag{14}$$

and

$$A(3, 1) = \frac{D_3}{\Lambda^2}, \tag{15}$$

are introduced, where D_2 and D_3 are diffusion coefficients for the 2^3S and 2^1S levels, respectively, and Λ is the characteristic diffusion length with $\Lambda = R/2.405$. In the present calculation, the values by Phelps[37] are used for D_2 and D_3.

Since radiation imprisonment takes place for the resonance transitions from all ^1P levels to the ground level in the range of filling pressure of interest, $A(i, 1)$ for $i \geq 5$ must be multiplied by an escape factor[38,39]; $1.60/[k_0 R\{\pi \log (k_0 R)\}^{1/2}]$. Here k_0 is the maximum absorption coefficient and is described by $n(1)$, T_{gas} and the oscillator strength when the Doppler broadening alone is present.

When p, R, and T_{gas} are given, the population coefficients $r_0(i)$ and $r_1(i)$ are calculated for the new coefficients $A(i, 1)$ for $i \geq 2$. In addition T_{ion} is given and then we can solve the plasma balance equation (9) and Eq. (2) simultaneously so that a relation among n_e, T_e and $n(i)$'s is obtained.

The calculation is carried out for a column of the radius $R = 1.6$ mm at $T_{\text{gas}} = T_{\text{ion}} = 723$ °K. The ranges of parameters are $2 \leq p \leq 8$ Torr and $10^9 \leq n_e \leq 3 \times 10^{13}$ cm^{-3}.

4. Results and Discussions

Examples of the results of the calculations are shown in Figs. 5~12 for $T_{\text{gas}} = 723$ °K and $R = 1.6$ mm. Figure 5 gives T_e as a function of n_e at $p = 2$, 4 and 8 Torr and it is seen that as either n_e or p increases T_e decreases. Figure 6 gives $n(i)$'s of several excited levels as a function of n_e at $p = 4$ and 8 Torr. In general, as n_e increases $n(i)$'s increase and saturate at some high values of n_e, but $n(2^3S)$ and $n(2^1S)$ decrease after the maximum at $n_e \simeq 5 \times 10^{11}$ cm^{-3}. In Fig. 7 the ratio $n(i)S(i)/Z$ in Eq. (11) is given as a function of n_e at $p = 4$ Torr. The ionization

takes place mainly from the ground level for $n_e \lesssim 10^{11}$ cm^{-3}, but as n_e increases the contributions from the excited levels gradually increase and become dominant for $n_e \gtrsim 10^{12}$ cm^{-3}. Further, the increases in the contributions from the four lowest excited levels begin at $n_e \simeq 10^{11}$ cm^{-3} and those from the higher levels $i \geq 6$ begin at $n_e \simeq 10^{12}$ cm^{-3}.

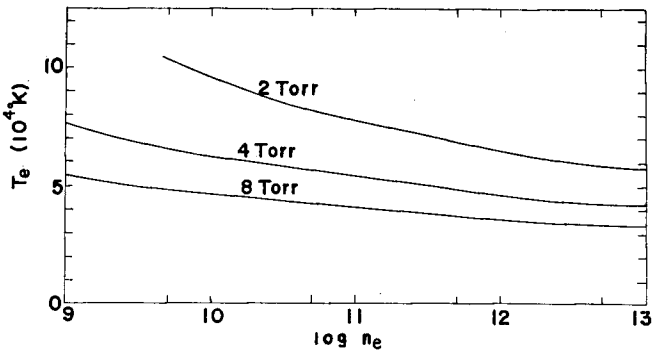

Fig. 5. Electron temperature T_e (°K) versus electron density n_e (cm^{-3}) for various filling pressures in the case of ambipolar diffusion with $R=1.6$ mm and $T_{gas}=T_{ion}=723$ °K.

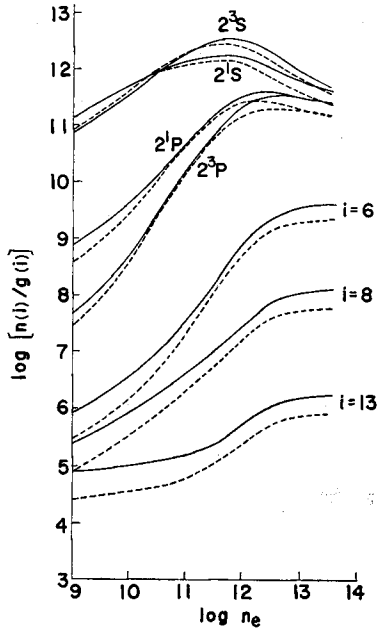

Fig. 6. Population densities versus electron density n_e(cm^{-3}) in the case of ambipolar diffusion with $R=1.6$ mm and $T_{gas}=T_{ion}=723$ °K. ——; 4 Torr. - - -; 8 Torr.

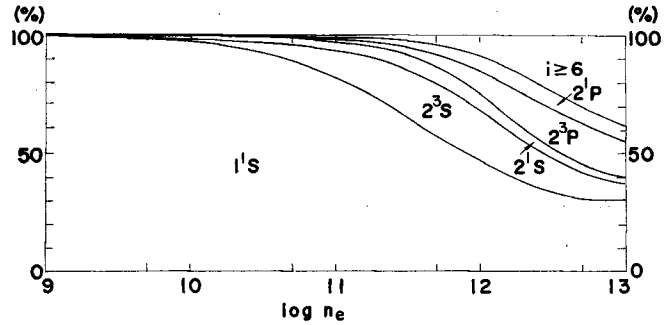

Fig. 7. Ratios fo ionization rates from various levels versus electron density $n_e(\mathrm{cm}^{-3})$ in the case of ambipolar diffusion with $R=1.6$ mm, $T_{\mathrm{gas}}=T_{\mathrm{ion}}=723$ °K and $p=4$ Torr.

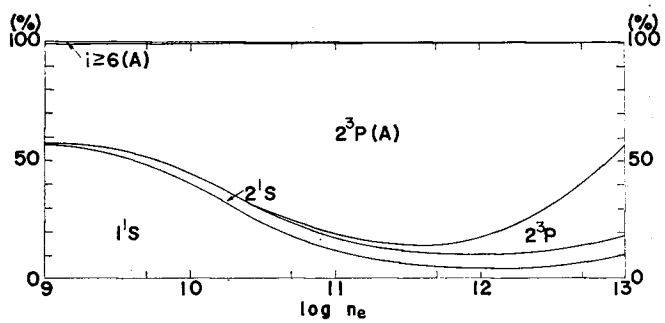

(a)

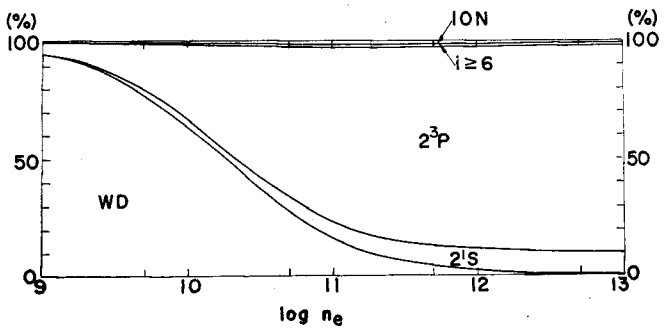

(b)

Fig. 8. Ratios of various rates for (a) population to or (b) depopulation from the 2^3S level versus electron density $n_e(\mathrm{cm}^{-3})$ in the same conditions as those of Fig. 7. Each level notation reprsesents the level (a) from or (b) to which transition takes place. A; radiative transition. ION; ionization. WD; wall diffusion. Otherwise; transition by electron collision.

In (a) and (b) of Figs. 8~12 the rate of population to and the rate of depopulation from the level i are indicated in the percent ratio to the total rate, respectively, at $p=4$ Torr. As shown in Fig. 8, for $n_e \lesssim 2\times10^{10}$ cm^{-3} the 2^3S level is populated by the collisional excitation from the ground level as well as by the cascading from the 2^3P level, while the level is depleted by the wall diffusion. As n_e increases from 2×10^{10} cm^{-3}, the radiative population from, and the collisional depopulation to the 2^3P level become large and almost balance between $n_e \simeq 10^{11}$ and 10^{12} cm^{-3}. Further, for $n_e \gtrsim 10^{12}$ cm^{-3} the collisional population from the 2^3P level increases.

In Fig. 9(a) the dominant population process to the 2^3P level is the collisional excitation from the 2^3S level except for the range of $n_e \lesssim 5\times10^9$ cm^{-3}, in which the population results from the direct excitation from the ground level and the cascading from higher levels $i \geq 6$. On the other hand, in Fig. 9(b) the dominant depopulation process from the 2^3P level is the radiative transition to the

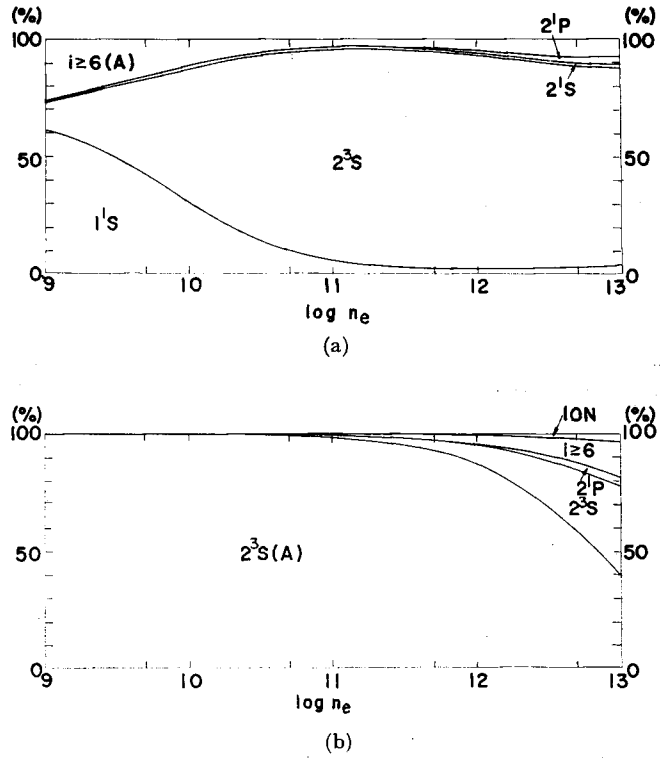

Fig. 9. Ratios of various rates for (a) population to or (b) depopulation from the 2^3P level versus electron density n_e(cm^{-3}) in the same conditions as those of Fig. 7. Each level notation represents the level (a) from or (b) to which transition takes place. A; radiative transition. ION; ionization. Otherwise; transition by electron collision.

2^3S level except for the range of $n_e \gtrsim 5 \times 10^{12}$ cm^{-3}, in which the collisional depopulations to the 2^3S level and higher levels $i \geq 6$ increase. The coronal equilibrium between the 2^3P and 2^3S levels is almost completely established between $n_e \simeq 10^{11}$ and 10^{12} cm^{-3}.

In Fig. 10(a) for $n_e \lesssim 10^{11}$ cm^{-3} the dominant processes of the populations to the 2^1S level are the direct excitation from the ground level and the cascading from the 2^1P level. For $n_e \gtrsim 10^{11}$ cm^{-3} the 2^3S level takes the place of the ground level. Further, for $n_e \gtrsim 2 \times 10^{12}$ cm^{-3} the collisional deexcitation from 2^1P to the 2^1S level takes the place of the cascading from the 2^1P level. In Fig. 10(b) for $n_e \lesssim 2 \times 10^{10}$ cm^{-3} the dominant processes of the depopulations from the 2^1S level are the wall diffusion. For $n_e \gtrsim 2 \times 10^{10}$ cm^{-3} the dominant processes of the depopulations from the 2^1S level change to the collisional transitions, in particular, the collisional excitation to the 2^1P level.

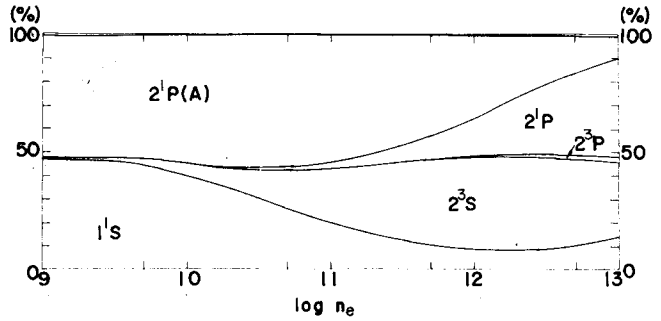

(a)

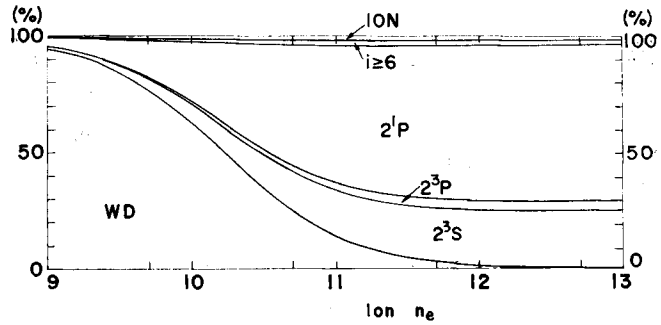

(b)

Fig. 10. Ratios of various rates for (a) population to or (b) depopulation from the 2^1S level versus electron density n_e(cm^{-3}) in the same conditions as those of Fig. 7. Each level notation represents the level (a) from or (b) to which transition takes place. A; radiative transition. ION; ionization. WD; wall diffusion. Otherwise; transition by electron collision.

In Figs. 11(a) and (b) for $n_e \lesssim 2\times10^{10}\,\mathrm{cm}^{-3}$ the dominant population and depopulation processes of the 2^1P level are the direct excitation from the ground level and the radiative transitions to the lower levels, respectively. Hence the 2^1P level is in the coronal equilibrium with the ground level. For $n_e \gtrsim 2\times10^{10}\,\mathrm{cm}^{-3}$, the dominant population process of the 2^1P level changes to the collisional excitation from the 2^1S level, and so the 2^1P level is in the coronal equilibrium with the 2^1S level. For $n_e \gtrsim 2\times10^{12}\,\mathrm{cm}^{-3}$, the dominant depopulation processes from the 2^1P level become the collisional transitions, in particular, the deexcitation to the 2^1S level.

As shown in Fig. 12, for $n_e \lesssim 10^{11}\,\mathrm{cm}^{-3}$ the level $i=8$ is populated mainly by the collisional excitation from the ground level, while the level is depleted by the radiative transition to lower levels. As n_e increases from $10^{11}\,\mathrm{cm}^{-3}$, the collisional population, in particular, from the level $i=7$ and the collisional depopulation to

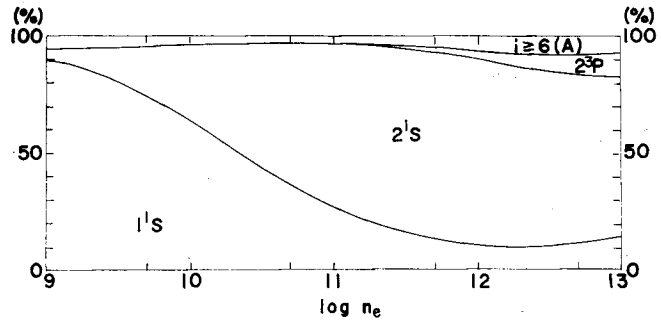

(a)

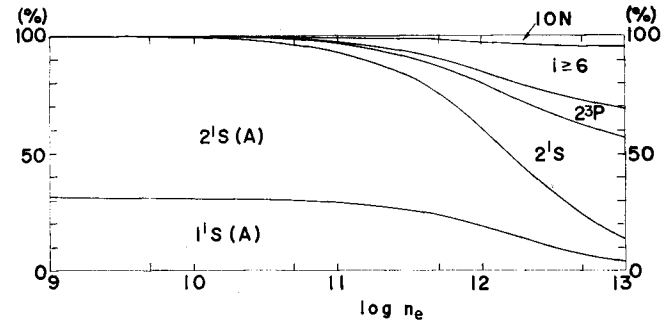

(b)

Fig. 11. Ratios of various rates for (a) population to or (b) depopulation from the 2^1P level versus electron density $n_e(\mathrm{cm}^{-3})$ in the same conditions as those of Fig. 7. Each level notation represents the level (a) from or (b) to which transition takes place. A; radiative transition. ION; ionization. Otherwise; transition by electron collision.

the higher adjacent level $i=9$ become large and balance each other; that is, the level 8 is almost governed by the stepwise excitation for $n_e \gtrsim 10^{11}$ cm^{-3}.

From the above results it is seen that the population and depopulation processes between the 2^3P and 2^3S levels are similar to those between the 2^1P and 2^1S levels. Further, both the singlet and triplet two-level systems are almost independent of each other in the low density range up to $n_e \simeq 10^{11}$ cm^{-3}. However, as n_e increases, the intercombination transitions between the two systems are induced to some extent by electronic collision, and the detailed balancing is almost realized between 2^3S and 2^1S as well as between 2^3P and 2^1P.

Detailed analysis is desirable for the behaviors of the population densities of the four lowest excited levels in connection with the atomic processes. The analysis will be shown in the near future together with the calculation of helium-cadmium laser plasma in a positive column.

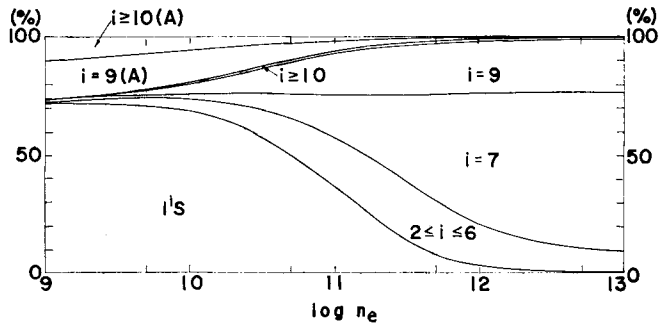

(a)

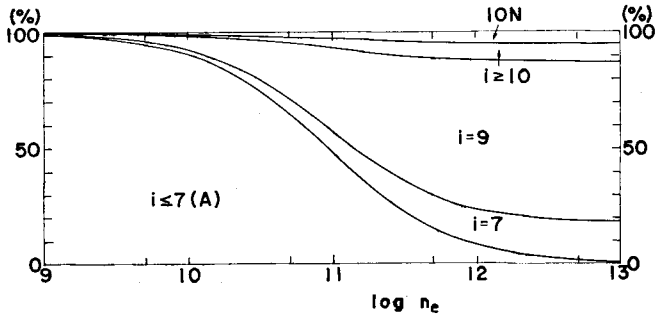

(b)

Fig. 12. Ratios of various rates for (a) population to or (b) depopulation from the level $i=8$ versus electron density n_e(cm^{-3}) in the same conditions as those of Fig. 7. Each level notation represents the level (a) from or (b) to which transition takes place. A; radiative transition. ION; ionization. Otherwise; transition by electron collision.

Table 2. Coefficients $A(i,j)$ in sec^{-1}.

j =	1 (1^1S)	2 (2^3S)	3 (2^1S)	4 (2^3P)	5 (2^1P)	6	7	8	9	10	11	12	13	14	15	16	17	18	19	20
i = 1 (1^1S)	–																			
2 (2^3S)	0	–																		
3 (2^1S)	0	0	–																	
4 (2^3P)	0	1.02^7	0	–																
5 (2^1P)	1.80^9	0	1.98^6	0	–															
6	4.71^7	2.37^6	1.12^6	3.17^7	9.63^6	–														
7	1.15^7	7.10^5	3.36^5	6.37^6	1.68^6	1.17^7	–													
8	3.84^6	2.64^5	1.13^5	1.88^6	4.84^5	2.62^6	3.56^6	–												
9	1.50^6	1.06^5	4.98^4	6.63^5	2.22^5	9.00^5	9.11^5	1.33^6	–											
10	7.76^5	5.10^4	1.99^4	3.40^5	7.67^3	3.82^5	3.48^5	3.83^5	5.89^5	–										
11	4.02^5	2.74^4	1.06^4	1.66^5	4.09^4	1.86^5	1.60^5	1.58^5	1.83^5	2.93^5	–									
12	2.19^5	1.53^4	6.02^3	9.49^4	1.94^4	1.00^5	8.31^4	7.72^4	8.00^4	9.64^4	1.59^5	–								
13	1.36^5	9.09^3	3.68^3	5.32^4	1.21^4	5.77^4	4.69^4	4.20^4	4.10^4	4.41^4	5.47^4	9.21^4	–							
14	8.06^4	9.48^3	3.16^3	2.84^4	9.48^3	3.52^4	2.82^4	2.47^4	2.32^4	2.35^4	2.59^4	3.29^4	5.63^4	–						
15	5.42^4	6.10^3	2.03^3	1.83^4	6.10^3	2.25^4	1.78^4	1.53^4	1.41^4	1.37^4	1.42^4	1.61^4	2.07^4	3.60^4	–					
16	4.27^4	4.07^3	1.36^3	1.22^4	4.07^3	1.49^4	1.17^4	9.96^3	8.98^3	8.53^3	8.53^3	9.05^3	1.04^4	1.36^4	2.39^4	–				
17	2.94^4	2.80^3	9.34^2	8.41^3	2.80^3	1.02^4	7.97^3	6.71^3	5.98^3	5.58^3	5.44^3	5.55^3	5.98^3	6.95^3	9.20^3	1.64^4	–			
18	2.08^4	1.98^3	6.60^2	5.94^3	1.98^3	7.20^3	5.58^3	4.67^3	4.11^3	3.79^3	3.62^3	3.60^3	3.73^3	4.08^3	4.80^3	6.41^3	1.15^4	–		
19	1.51^4	1.43^3	4.77^2	4.29^3	1.43^3	5.19^3	4.01^3	3.33^3	2.91^3	2.65^3	2.50^3	2.44^3	2.46^3	2.59^3	2.86^3	3.40^3	4.58^3	8.27^3	–	
20	1.11^4	1.05^3	3.51^2	3.16^3	1.05^3	3.82^3	2.94^3	2.43^3	2.11^3	1.91^3	1.78^3	1.71^3	1.70^3	1.73^3	1.84^3	2.05^3	2.46^3	3.34^3	6.07^3	–
21	8.36^3	7.91^2	2.64^2	2.37^3	7.91^2	2.86^3	2.19^3	1.80^3	1.56^3	1.40^3	1.30^3	1.23^3	1.21^3	1.21^3	1.25^3	1.34^3	1.51^3	1.82^3	2.48^3	4.54^3

Read : $1.02^7 = 1.02 \times 10^7$

Table 3. Absorption oscillators trength $f(i,j)$.

j =	1 (1^1S)	2 (2^3S)	3 (2^1S)	4 (2^3P)	5 (2^1P)	6	7	8	9	10	11	12	13	14	15	16	17	18	19	20
i = 1 (1^1S)	–																			
2 (2^3S)	0	–																		
3 (2^1S)	0	0	–																	
4 (2^3P)	0	5.39^{-1}	–	–																
5 (2^1P)	2.76^{-1}	0	3.76^{-1}	0	–															
6	7.34^{-2}	6.19^{-2}	1.53^{-1}	6.58^{-1}	7.50^{-1}	–														
7	3.01^{-2}	2.28^{-2}	5.08^{-2}	1.36^{-1}	1.30^{-1}	1.09	–													
8	1.53^{-2}	1.14^{-2}	2.21^{-2}	5.09^{-2}	4.65^{-2}	1.79^{-1}	1.34	–												
9	8.50^{-3}	6.09^{-3}	1.28^{-2}	2.32^{-2}	2.74^{-2}	6.44^{-2}	2.11^{-1}	1.59	–											
10	5.94^{-3}	3.81^{-3}	6.58^{-2}	1.53^{-2}	1.21^{-2}	3.14^{-2}	7.47^{-2}	2.43^{-1}	1.83	–										
11	4.00^{-3}	2.60^{-3}	4.42^{-3}	9.37^{-3}	8.06^{-3}	1.81^{-2}	3.62^{-2}	8.44^{-2}	2.74^{-1}	2.08	–									
12	2.75^{-3}	1.80^{-3}	3.10^{-3}	6.60^{-3}	4.71^{-3}	1.15^{-2}	2.08^{-2}	4.06^{-2}	9.39^{-2}	3.05^{-1}	2.32	–								
13	2.10^{-3}	1.31^{-3}	2.30^{-3}	4.49^{-3}	3.55^{-3}	7.79^{-3}	1.32^{-2}	2.32^{-2}	4.48^{-2}	1.03^{-1}	3.35^{-1}	2.57	–							
14	1.50^{-3}	1.63^{-3}	2.36^{-3}	2.86^{-3}	3.32^{-3}	5.56^{-3}	8.99^{-3}	1.47^{-2}	2.54^{-2}	4.88^{-2}	1.12^{-1}	3.66^{-1}	2.81	–						
15	1.20^{-3}	1.24^{-3}	1.79^{-3}	2.17^{-3}	2.52^{-3}	4.12^{-3}	6.45^{-3}	1.00^{-2}	1.61^{-2}	2.76^{-2}	5.28^{-2}	1.22^{-1}	3.97^{-1}	3.06	–					
16	1.11^{-3}	9.63^{-4}	1.39^{-3}	1.69^{-3}	1.95^{-3}	3.15^{-3}	4.80^{-3}	7.19^{-3}	1.10^{-2}	1.74^{-2}	2.97^{-2}	5.67^{-2}	1.31^{-1}	4.27^{-1}	3.30	–				
17	8.86^{-4}	7.65^{-4}	1.11^{-3}	1.34^{-3}	1.55^{-3}	2.46^{-3}	3.68^{-3}	5.37^{-3}	7.86^{-3}	1.18^{-2}	1.87^{-2}	3.18^{-2}	6.07^{-2}	1.40^{-1}	4.58^{-2}	3.54	–			
18	7.19^{-4}	6.18^{-4}	8.93^{-4}	1.08^{-3}	1.25^{-3}	1.96^{-3}	2.89^{-3}	4.13^{-3}	5.87^{-3}	8.47^{-3}	1.27^{-2}	1.99^{-2}	3.38^{-2}	6.45^{-2}	1.49^{-1}	4.89^{-1}	3.79	–		
19	5.92^{-4}	5.06^{-4}	7.32^{-4}	8.84^{-4}	1.02^{-3}	1.59^{-3}	2.32^{-3}	3.23^{-3}	4.51^{-3}	6.32^{-3}	9.05^{-3}	1.35^{-2}	2.11^{-2}	3.58^{-2}	6.82^{-2}	1.58^{-1}	5.19^{-1}	4.03	–	
20	4.93^{-4}	4.20^{-4}	6.07^{-4}	7.33^{-4}	8.47^{-4}	1.31^{-3}	1.89^{-3}	2.61^{-3}	3.56^{-3}	4.87^{-3}	6.75^{-3}	9.61^{-3}	1.42^{-2}	2.23^{-2}	3.78^{-2}	7.23^{-2}	1.67^{-1}	5.50^{-1}	4.28	–
21	4.15^{-4}	$3.53\bar{e}^{4}$	5.09^{-4}	6.15^{-4}	7.11^{-4}	1.09^{-3}	1.56^{-3}	2.13^{-3}	2.86^{-3}	3.84^{-3}	5.19^{-3}	7.15^{-3}	1.01^{-2}	1.50^{-2}	2.35^{-2}	3.98^{-2}	7.61^{-2}	1.76^{-1}	5.80^{-1}	4.52

Read : $5.39^{-1} = 5.39 \times 10^{-1}$

Table 4. Population confficients $r_0(i)$ for an optically thin helium plasma.

	i =	2 (2^3S)	3 (2^1S)	4 (2^3P)	5 (2^1P)	6	8	10	13	18
T_e = 8000 °K	log n_e									
	5	4.43^{7}	3.09^{7}	2.42^{-1}	1.44^{-3}	6.33^{-3}	2.65^{-2}	4.47^{-2}	6.61^{-2}	1.01^{-1}
	6	4.46^{6}	3.11^{6}	2.43^{-1}	1.45^{-3}	6.47^{-3}	2.73^{-2}	4.64^{-2}	6.99^{-2}	1.27^{-1}
	7	4.60^{5}	3.21^{5}	2.51^{-1}	1.49^{-3}	7.07^{-3}	3.05^{-2}	5.35^{-2}	8.78^{-2}	3.42^{-1}
	8	4.99^{4}	3.48^{4}	2.72^{-1}	1.60^{-3}	8.72^{-3}	3.95^{-2}	7.48^{-2}	1.73^{-1}	7.29^{-1}
	9	5.82^{3}	4.06^{3}	3.18^{-1}	1.84^{-3}	1.23^{-2}	6.02^{-2}	1.41^{-1}	5.20^{-1}	9.30^{-1}
	10	7.40^{2}	5.17^{2}	4.05^{-1}	2.30^{-3}	1.93^{-2}	1.11^{-1}	4.20^{-1}	8.50^{-1}	9.85^{-1}
	11	1.03^{2}	7.23^{1}	5.64^{-1}	3.18^{-3}	3.38^{-2}	3.17^{-1}	7.93^{-1}	9.66^{-1}	9.97^{-1}
	12	1.55^{1}	1.08^{1}	8.09^{-1}	4.99^{-3}	7.05^{-2}	7.13^{-1}	9.48^{-1}	9.93^{-1}	1.00
	13	1.99	1.44	7.38^{-1}	9.14^{-3}	2.15^{-1}	9.19^{-1}	9.88^{-1}	9.99^{-1}	1.00
	14	3.03^{-1}	2.34^{-1}	2.85^{-1}	2.05^{-2}	6.47^{-1}	9.80^{-1}	9.97^{-1}	1.00	1.00
	15	1.23^{-1}	1.08^{-1}	1.32^{-1}	5.75^{-2}	9.08^{-1}	9.96^{-1}	9.99^{-1}	1.00	1.00
	16	3.16^{-1}	3.09^{-1}	3.22^{-1}	2.86^{-1}	9.59^{-1}	9.98^{-1}	1.00	1.00	1.00
	17	7.45^{-1}	7.43^{-1}	7.48^{-1}	7.39^{-1}	9.86^{-1}	9.99^{-1}	1.00	1.00	1.00
	18	8.86^{-1}	8.86^{-1}	8.88^{-1}	8.88^{-1}	9.94^{-1}	1.00	1.00	1.00	1.00
	19	9.03^{-1}	9.04^{-1}	9.05^{-1}	9.06^{-1}	9.95^{-1}	1.00	1.00	1.00	1.00
T_e = 16000 °K	5	1.01^{9}	4.70^{8}	7.62	2.87^{-2}	3.10^{-2}	5.67^{-2}	7.43^{-2}	9.32^{-2}	1.22^{-1}
	6	1.01^{8}	4.72^{7}	7.65	2.88^{-2}	3.14^{-2}	5.76^{-2}	7.59^{-2}	9.66^{-2}	1.43^{-1}
	7	1.03^{7}	4.79^{6}	7.76	2.92^{-2}	3.29^{-2}	6.16^{-2}	8.33^{-2}	1.13^{-1}	3.28^{-1}
	8	1.07^{6}	5.00^{5}	8.10	3.03^{-2}	3.73^{-2}	7.33^{-2}	1.06^{-1}	1.90^{-1}	7.11^{-1}
	9	1.17^{5}	5.44^{4}	8.81	3.27^{-2}	4.68^{-2}	1.00^{-1}	1.74^{-1}	5.17^{-1}	9.24^{-1}
	10	1.34^{4}	6.23^{3}	1.01^{1}	3.71^{-2}	6.49^{-2}	1.63^{-1}	4.47^{-1}	8.50^{-1}	9.85^{-1}
	11	1.62^{3}	7.56^{2}	1.22^{1}	4.46^{-2}	1.00^{-1}	3.90^{-1}	8.11^{-1}	9.67^{-1}	9.97^{-1}
	12	1.94^{2}	9.14^{1}	1.37^{1}	5.74^{-2}	1.87^{-1}	7.70^{-1}	9.57^{-1}	9.94^{-1}	1.00
	13	1.75^{1}	8.74	7.80	7.62^{-2}	4.64^{-1}	9.47^{-1}	9.92^{-1}	9.99^{-1}	1.00
	14	1.86	1.05	1.78	1.13^{-1}	8.49^{-1}	9.91^{-1}	9.99^{-1}	1.00	1.00
	15	6.01^{-1}	4.48^{-1}	6.39^{-1}	2.61^{-1}	9.64^{-1}	9.98^{-1}	1.00	1.00	1.00
	16	8.04^{-1}	7.63^{-1}	8.15^{-1}	7.15^{-1}	9.90^{-1}	1.00	1.00	1.00	1.00
	17	9.65^{-1}	9.59^{-1}	9.67^{-1}	9.54^{-1}	9.98^{-1}	1.00	1.00	1.00	1.00
	18	9.88^{-1}	9.88^{-1}	9.89^{-1}	9.88	1.00	1.00	1.00	1.00	1.00
	19	9.91^{-1}	9.91^{-1}	9.92^{-1}	9.92^{-1}	1.00	1.00	1.00	1.00	1.00
T_e = 32000 °K	5	6.88^{9}	2.12^{9}	6.42^{1}	1.51^{-1}	9.38^{-2}	9.92^{-2}	1.10^{-1}	1.24^{-1}	1.46^{-1}
	6	6.89^{8}	2.12^{8}	6.43^{1}	1.52^{-1}	9.43^{-2}	1.00^{-1}	1.12^{-1}	1.27^{-1}	1.62^{-1}
	7	6.94^{7}	2.14^{7}	6.48^{1}	1.53^{-1}	9.67^{-2}	1.04^{-1}	1.19^{-1}	1.42^{-1}	3.16^{-1}
	8	7.10^{6}	2.18^{6}	6.63^{1}	1.56^{-1}	1.04^{-1}	1.17^{-1}	1.41^{-1}	2.08^{-1}	6.89^{-1}
	9	7.43^{5}	2.29^{5}	6.94^{1}	1.62^{-1}	1.19^{-1}	1.46^{-1}	2.05^{-1}	5.06^{-1}	9.17^{-1}
	10	8.02^{4}	2.47^{4}	7.49^{1}	1.74^{-1}	1.49^{-1}	2.13^{-1}	4.59^{-1}	8.43^{-1}	8.83^{-1}
	11	8.79^{3}	2.71^{3}	8.15^{1}	1.92^{-1}	2.10^{-1}	4.36^{-1}	8.16^{-1}	9.67^{-1}	9.97^{-1}
	12	8.30^{2}	2.62^{2}	7.12^{1}	2.08^{-1}	3.95^{-1}	8.01^{-1}	9.61^{-1}	9.94^{-1}	1.00
	13	4.78^{1}	1.69^{1}	2.34^{1}	2.03^{-1}	7.63^{-1}	9.64^{-1}	9.90^{-1}	9.99^{-1}	1.00
	14	3.94	1.67	3.65	2.35^{-1}	9.50^{-1}	9.95^{-1}	9.99^{-1}	1.00	1.00
	15	1.09	7.07^{-1}	1.11	4.60^{-1}	9.86^{-1}	9.99^{-1}	1.00	1.00	1.00
	16	9.74^{-1}	9.06^{-1}	9.81^{-1}	8.62^{-1}	9.97^{-1}	1.00	1.00	1.00	1.00
	17	9.94^{-1}	9.86^{-1}	9.95^{-1}	9.82^{-1}	1.00	1.00	1.00	1.00	1.00
	18	9.97^{-1}	9.96^{-1}	9.98^{-1}	9.96^{-1}	1.00	1.00	1.00	1.00	1.00
	19	9.97^{-1}	9.97^{-1}	9.98^{-1}	9.98^{-1}	1.00	1.00	1.00	1.00	1.00

Read : $4.43^{7} = 4.43 \times 10^{7}$

Table 4. (Continued).

	i =	2 (2^3S)	3 (2^1S)	4 (2^3P)	5 (2^1P)	6	8	10	13	18
T_e = 50000 °K	log n_e									
	5	1.54^{10}	3.77^{9}	1.56^{2}	2.88^{-1}	1.66^{-1}	1.36^{-1}	1.39^{-1}	1.48^{-1}	1.65^{-1}
	6	1.55^{9}	3.78^{8}	1.56^{2}	2.89^{-1}	1.67^{-1}	1.37^{-1}	1.40^{-1}	1.51^{-1}	1.79^{-1}
	7	1.55^{8}	3.80^{7}	1.57^{2}	2.90^{-1}	1.69^{-1}	1.41^{-1}	1.47^{-1}	1.64^{-1}	3.13^{-1}
	8	1.58^{7}	3.85^{6}	1.59^{2}	2.94^{-1}	1.77^{-1}	1.53^{-1}	1.68^{-1}	2.23^{-1}	6.75^{-1}
	9	1.63^{6}	3.97^{5}	1.64^{2}	3.02^{-1}	1.96^{-1}	1.83^{-1}	2.28^{-1}	4.99^{-1}	9.11^{-1}
	10	1.71^{5}	4.18^{4}	1.73^{2}	3.16^{-1}	2.31^{-1}	2.48^{-1}	4.64^{-1}	8.37^{-1}	9.82^{-1}
	11	1.78^{4}	4.38^{3}	1.79^{2}	3.36^{-1}	3.16^{-1}	4.62^{-1}	8.15^{-1}	9.66^{-1}	9.97^{-1}
	12	1.45^{3}	3.68^{2}	1.33^{2}	3.33^{-1}	5.95^{-1}	8.17^{-1}	9.62^{-1}	9.94^{-1}	1.00
	13	6.62^{1}	2.00^{1}	3.29^{1}	2.93^{-1}	9.45^{-1}	9.72^{-1}	9.95^{-1}	9.99^{-1}	1.00
	14	5.04	1.92	4.52	3.15^{-1}	9.89^{-1}	9.97^{-1}	9.99^{-1}	1.00	1.00
	15	1.28	8.03^{-1}	1.28	5.56^{-1}	9.93^{-1}	9.99^{-1}	1.00	1.00	1.00
	16	1.01	9.39^{-1}	1.02	9.01^{-1}	9.98^{-1}	1.00	1.00	1.00	1.00
	17	1.00	9.91^{-1}	1.00	9.88^{-1}	1.00	1.00	1.00	1.00	1.00
	18	9.99^{-1}	9.98^{-1}	9.99^{-1}	9.98^{-1}	1.00	1.00	1.00	1.00	1.00
	19	9.99^{-1}	9.98^{-1}	9.99^{-1}	9.99^{-1}	1.00	1.00	1.00	1.00	1.00
T_e = 64000 °K	5	2.18^{10}	4.76^{9}	2.25^{2}	3.74^{-1}	2.18^{-1}	1.60^{-1}	1.57^{-1}	1.64^{-1}	1.78^{-1}
	6	2.18^{9}	4.76^{8}	2.26^{2}	3.74^{-1}	2.18^{-1}	1.61^{-1}	1.59^{-1}	1.66^{-1}	1.90^{-1}
	7	2.19^{8}	4.78^{7}	2.27^{2}	3.76^{-1}	2.21^{-1}	1.65^{-1}	1.65^{-1}	1.79^{-1}	3.13^{-1}
	8	2.21^{7}	4.84^{6}	2.29^{2}	3.80^{-1}	2.30^{-1}	1.77^{-1}	1.85^{-1}	2.34^{-1}	6.67^{-1}
	9	2.27^{6}	4.96^{5}	2.35^{2}	3.88^{-1}	2.49^{-1}	2.06^{-1}	2.43^{-1}	4.96^{-1}	9.08^{-1}
	10	2.36^{5}	5.17^{4}	2.45^{2}	4.03^{-1}	2.88^{-1}	2.70^{-1}	4.67^{-1}	8.33^{-1}	9.81^{-1}
	11	2.41^{4}	5.29^{3}	2.47^{2}	4.21^{-1}	3.86^{-1}	4.76^{-1}	8.15^{-1}	9.65^{-1}	9.97^{-1}
	12	1.82^{3}	4.19^{2}	1.70^{2}	4.04^{-1}	7.20^{-1}	8.25^{-1}	9.63^{-1}	9.94^{-1}	1.00
	13	7.64^{1}	2.16^{1}	3.79^{1}	3.47^{-1}	1.04	9.77^{-1}	9.96^{-1}	9.99^{-1}	1.00
	14	5.64	2.09	4.96	3.65^{-1}	1.01	9.98^{-1}	1.00	1.00	1.00
	15	1.36	8.52^{-1}	1.34	6.02^{-1}	9.96^{-1}	1.00	1.00	1.00	1.00
	16	1.03	9.51^{-1}	1.03	9.16^{-1}	9.99^{-1}	1.00	1.00	1.00	1.00
	17	1.00	9.93^{-1}	1.00	9.90^{-1}	1.00	1.00	1.00	1.00	1.00
	18	9.99^{-1}	9.98^{-1}	9.99^{-1}	9.98^{-1}	1.00	1.00	1.00	1.00	1.00
	19	9.99^{-1}	9.98^{-1}	9.99^{-1}	9.99^{-1}	9.99^{-1}	1.00	1.00	1.00	1.00
T_e = 128000 °K	5	4.49^{10}	7.66^{9}	4.66^{2}	6.30^{-1}	4.03^{-1}	2.41^{-1}	2.19^{-1}	2.15^{-1}	2.22^{-1}
	6	4.49^{9}	7.66^{8}	4.66^{2}	6.30^{-1}	4.04^{-1}	2.42^{-1}	2.19^{-1}	2.17^{-1}	2.30^{-1}
	7	4.50	7.67	4.67	6.31^{-1}	4.07^{-1}	2.45^{-1}	2.25^{-1}	2.27^{-1}	3.25^{-1}
	8	4.52^{7}	7.72^{6}	4.70^{2}	6.35^{-1}	4.15^{-1}	2.56^{-1}	2.42^{-1}	2.72^{-1}	6.50^{-1}
	9	4.59^{6}	7.83^{5}	4.76^{2}	6.43^{-1}	4.36^{-1}	2.83^{-1}	2.92^{-1}	4.94^{-1}	8.99^{-1}
	10	4.67^{5}	7.98^{4}	4.85^{2}	6.56^{-1}	4.80^{-1}	3.41^{-1}	4.82^{-1}	8.24^{-1}	9.79^{-1}
	11	4.56^{4}	7.85^{3}	4.68^{2}	6.66^{-1}	6.16^{-1}	5.21^{-1}	8.13^{-1}	9.62^{-1}	9.97^{-1}
	12	3.06^{3}	5.73^{2}	2.85^{2}	6.21^{-1}	1.10	8.49^{-1}	9.64^{-1}	9.94^{-1}	1.00
	13	1.14^{2}	2.96^{1}	5.41^{1}	5.32^{-1}	1.31	9.89^{-1}	9.97^{-1}	1.00	1.00
	14	7.96	2.88	6.46	5.28^{-1}	1.06	1.00	1.00	1.00	1.00
	15	1.62	1.01	1.52	7.23^{-1}	1.00	1.00	1.00	1.00	1.00
	16	1.06	9.81^{-1}	1.05	9.46^{-1}	1.00	1.00	1.00	1.00	1.00
	17	1.01	9.96^{-1}	1.00	9.93^{-1}	1.00	1.00	1.00	1.00	1.00
	18	1.00	9.98^{-1}	1.00	9.99^{-1}	1.00	1.00	1.00	1.00	1.00
	19	9.99^{-1}	9.98^{-1}	1.00	9.99^{-1}	1.00	1.00	1.00	1.00	1.00

Read : $1.54^{10} = 1.54 \times 10^{10}$

Table 5. Population coefficients $r_1(i)$ for an optically thin helium plasma.

	i =	2 (2^3S)	3 (2^1S)	4 (2^3P)	5 (2^1P)	6	8	10	13	18
T_e = 8000 °K	log n_e									
	5	1.66^{-2}	1.17^{-2}	7.88^{-11}	4.03^{-13}	3.05^{-14}	8.99^{-15}	6.35^{-15}	5.42^{-15}	5.07^{-15}
	6	1.66^{-2}	1.17^{-2}	7.88^{-10}	4.03^{-12}	3.05^{-13}	8.99^{-14}	6.34^{-14}	5.41^{-14}	4.92^{-14}
	7	1.66^{-2}	1.17^{-2}	7.88^{-9}	4.03^{-11}	3.05^{-12}	8.97^{-13}	6.31^{-13}	5.34^{-13}	3.78^{-13}
	8	1.66^{-2}	1.17^{-2}	7.88^{-8}	4.03^{-10}	3.05^{-11}	8.92^{-12}	6.18^{-12}	4.94^{-12}	1.64^{-12}
	9	1.66^{-2}	1.17^{-2}	7.88^{-7}	4.03^{-9}	3.05^{-10}	8.79^{-11}	5.78^{-11}	2.93^{-11}	4.37^{-12}
	10	1.65^{-2}	1.17^{-2}	7.87^{-6}	4.03^{-8}	3.09^{-9}	8.46^{-10}	4.09^{-10}	9.67^{-11}	9.40^{-12}
	11	1.64^{-2}	1.16^{-2}	7.78^{-5}	4.03^{-7}	3.49^{-8}	7.10^{-9}	1.73^{-9}	2.65^{-10}	2.11^{-11}
	12	1.55^{-2}	1.10^{-2}	6.96^{-4}	4.02^{-6}	7.04^{-7}	5.56^{-8}	8.52^{-9}	1.07^{-9}	7.70^{-11}
	13	1.14^{-2}	8.37^{-3}	3.40^{-3}	3.99^{-5}	1.98^{-5}	9.10^{-7}	1.19^{-7}	1.41^{-8}	9.73^{-10}
	14	8.49^{-3}	6.55^{-3}	5.80^{-3}	3.93^{-4}	1.38^{-4}	5.97^{-6}	7.69^{-7}	8.98^{-8}	6.19^{-9}
	15	1.11^{-2}	9.41^{-3}	9.33^{-3}	3.76^{-3}	3.74^{-4}	1.60^{-5}	2.06^{-6}	2.41^{-7}	1.66^{-8}
	16	3.36^{-2}	3.22^{-2}	3.18^{-2}	2.75^{-2}	1.53^{-3}	6.76^{-5}	8.70^{-6}	1.01^{-6}	6.99^{-8}
	17	7.85^{-2}	7.76^{-2}	7.61^{-2}	7.46^{-2}	3.96^{-3}	1.69^{-4}	2.18^{-5}	2.54^{-6}	1.75^{-7}
	18	9.31^{-2}	9.24^{-2}	9.10^{-2}	9.00^{-2}	4.74^{-3}	2.02^{-4}	2.60^{-5}	3.04^{-6}	2.09^{-7}
	19	9.49^{-2}	9.43^{-2}	9.28^{-2}	9.19^{-2}	4.84^{-3}	2.07^{-4}	2.66^{-5}	3.10^{-6}	2.14^{-7}
T_e = 16000 °K	5	9.17^{-3}	4.53^{-3}	6.33^{-11}	2.16^{-13}	2.78^{-14}	9.34^{-15}	6.83^{-15}	5.78^{-15}	5.30^{-15}
	6	9.17^{-3}	4.53^{-3}	6.33^{-10}	2.16^{-12}	2.78^{-13}	9.33^{-14}	6.82^{-14}	5.76^{-14}	5.17^{-14}
	7	9.17^{-3}	4.53^{-3}	6.33^{-9}	2.16^{-11}	2.78^{-12}	9.31^{-13}	6.78^{-13}	5.69^{-13}	4.11^{-13}
	8	9.17^{-3}	4.53^{-3}	6.33^{-8}	2.16^{-10}	2.78^{-11}	9.23^{-12}	6.63^{-12}	5.28^{-12}	1.86^{-12}
	9	9.17^{-3}	4.53^{-3}	6.33^{-7}	2.16^{-9}	2.78^{-10}	9.05^{-11}	6.17^{-11}	3.22^{-11}	5.02^{-12}
	10	9.16^{-3}	4.53^{-3}	6.32^{-6}	2.15^{-8}	2.82^{-9}	8.60^{-10}	4.30^{-10}	1.06^{-10}	1.06^{-11}
	11	9.05^{-3}	4.48^{-3}	6.20^{-5}	2.15^{-7}	3.31^{-8}	6.96^{-9}	1.74^{-9}	2.73^{-10}	2.23^{-10}
	12	8.20^{-3}	4.12^{-3}	5.23^{-4}	2.10^{-6}	7.40^{-7}	5.34^{-8}	8.17^{-9}	1.04^{-9}	7.59^{-11}
	13	5.34^{-3}	2.91^{-3}	2.01^{-3}	1.92^{-5}	1.55^{-5}	6.51^{-7}	8.45^{-8}	9.95^{-9}	6.96^{-10}
	14	3.78^{-3}	2.31^{-3}	2.78^{-3}	1.71^{-4}	5.80^{-5}	2.27^{-6}	2.89^{-7}	3.37^{-8}	2.34^{-9}
	15	4.41^{-3}	3.24^{-3}	3.69^{-3}	1.39^{-3}	1.06^{-4}	4.10^{-6}	5.20^{-7}	6.07^{-8}	4.22^{-9}
	16	7.20^{-3}	6.53^{-3}	6.38^{-3}	5.27^{-3}	2.20^{-4}	8.48^{-6}	1.08^{-6}	1.25^{-7}	8.70^{-9}
	17	8.68^{-3}	8.28^{-3}	7.80^{-3}	7.32^{-3}	2.80^{-4}	1.08^{-5}	1.37^{-6}	1.59^{-7}	1.10^{-8}
	18	8.90^{-3}	8.53^{-3}	8.01^{-3}	7.61^{-3}	2.88^{-4}	1.11^{-5}	1.41^{-6}	1.64^{-7}	1.14^{-8}
	19	8.92^{-3}	8.56^{-3}	8.03^{-3}	7.64^{-3}	2.89^{-4}	1.11^{-5}	1.41^{-6}	1.64^{-7}	1.14^{-8}
T_e = 32000 °K	5	7.62^{-3}	2.69^{-3}	6.74^{-11}	1.62^{-13}	3.59^{-14}	1.30^{-14}	9.70^{-15}	8.17^{-15}	7.43^{-15}
	6	7.62^{-3}	2.69^{-3}	6.74^{-10}	1.62^{-12}	3.59^{-13}	1.30^{-13}	9.68^{-14}	8.15^{-14}	7.29^{-14}
	7	7.62^{-3}	2.69^{-3}	6.74^{-9}	1.62^{-11}	3.59^{-12}	1.30^{-12}	9.63^{-13}	8.05^{-13}	6.01^{-13}
	8	7.62^{-3}	2.69^{-3}	6.74^{-8}	1.62^{-10}	3.58^{-11}	1.29^{-11}	9.42^{-12}	7.53^{-12}	2.86^{-12}
	9	7.61^{-3}	2.69^{-3}	6.73^{-7}	1.62^{-9}	3.57^{-10}	1.26^{-10}	8.78^{-11}	4.80^{-11}	7.98^{-12}
	10	7.58^{-3}	2.68^{-3}	6.70^{-6}	1.62^{-8}	3.63^{-9}	1.19^{-9}	6.20^{-10}	1.62^{-10}	1.69^{-11}
	11	7.37^{-3}	2.62^{-3}	6.45^{-5}	1.60^{-7}	4.34^{-8}	9.52^{-9}	2.49^{-9}	4.06^{-10}	3.42^{-11}
	12	5.93^{-3}	2.21^{-3}	4.72^{-4}	1.48^{-6}	9.23^{-7}	6.82^{-8}	1.07^{-8}	1.40^{-9}	1.05^{-10}
	13	2.92^{-3}	1.36^{-3}	1.21^{-3}	1.18^{-5}	1.19^{-5}	5.19^{-7}	6.89^{-8}	8.25^{-9}	5.87^{-10}
	14	1.92^{-3}	1.12^{-3}	1.35^{-3}	9.75^{-5}	2.91^{-5}	1.18^{-6}	1.53^{-7}	1.81^{-8}	1.28^{-9}
	15	2.01^{-3}	1.51^{-3}	1.54^{-3}	6.68^{-4}	4.35^{-5}	1.73^{-6}	2.24^{-7}	2.64^{-8}	1.86^{-9}
	16	2.40^{-3}	2.29^{-3}	1.89^{-3}	1.68^{-3}	6.32^{-5}	2.50^{-6}	3.22^{-7}	3.80^{-8}	2.68^{-9}
	17	2.51^{-3}	2.52^{-3}	2.00^{-3}	1.99^{-3}	6.90^{-5}	2.72^{-6}	3.51^{-7}	4.14^{-8}	2.92^{-9}
	18	2.53^{-3}	2.54^{-3}	2.01^{-3}	2.02^{-3}	6.97^{-5}	2.75^{-6}	3.55^{-7}	4.18^{-8}	2.95^{-9}
	19	2.53^{-3}	2.55^{-3}	2.01^{-3}	2.03^{-3}	6.98^{-5}	2.75^{-6}	3.55^{-7}	4.19^{-8}	2.95^{-9}

Read : $1.66^{-2} = 1.66 \times 10^{-2}$

Table 5. (Continued.)

	i =	2 (2^3S)	3 (2^1S)	4 (2^3P)	5 (2^1P)	6	8	10	13	18
T_e = 50000 °K	log n_e									
	5	6.74^{-3}	2.04^{-3}	6.52^{-11}	1.44^{-13}	4.23^{-14}	1.62^{-14}	1.22^{-14}	1.03^{-14}	9.30^{-15}
	6	6.74^{-3}	2.04^{-3}	6.52^{-10}	1.44^{-12}	4.23^{-13}	1.62^{-13}	1.22^{-13}	1.03^{-13}	9.15^{-14}
	7	6.74^{-3}	2.04^{-3}	6.52^{-9}	1.44^{-11}	4.23^{-12}	1.62^{-12}	1.21^{-12}	1.02^{-12}	7.72^{-13}
	8	6.73^{-3}	2.04^{-3}	6.52^{-8}	1.43^{-10}	4.22^{-11}	1.60^{-11}	1.19^{-11}	9.55^{-12}	3.80^{-12}
	9	6.72^{-3}	2.04^{-3}	6.51^{-7}	1.43^{-9}	4.21^{-10}	1.57^{-10}	1.11^{-10}	6.30^{-11}	1.09^{-11}
	10	6.68^{-3}	2.03^{-3}	6.46^{-6}	1.43^{-8}	4.25^{-9}	1.48^{-9}	7.97^{-10}	2.17^{-10}	2.32^{-11}
	11	6.39^{-3}	1.96^{-3}	6.11^{-5}	1.41^{-7}	5.00^{-8}	1.18^{-8}	3.20^{-9}	5.38^{-10}	4.61^{-11}
	12	4.63^{-3}	1.57^{-3}	3.97^{-4}	1.27^{-6}	9.47^{-7}	7.60^{-8}	1.24^{-8}	1.65^{-9}	1.25^{-10}
	13	1.96^{-3}	9.73^{-4}	8.18^{-4}	1.01^{-5}	9.41^{-6}	4.35^{-8}	5.90^{-8}	7.19^{-9}	5.18^{-10}
	14	1.27^{-3}	8.60^{-4}	8.44^{-4}	8.52^{-5}	2.02^{-5}	8.57^{-7}	1.13^{-7}	1.36^{-8}	9.72^{-10}
	15	1.31^{-3}	1.18^{-3}	9.31^{-4}	5.40^{-4}	2.95^{-5}	1.23^{-7}	1.61^{-7}	1.93^{-8}	1.38^{-9}
	16	1.46^{-3}	1.66^{-3}	1.07^{-3}	1.19^{-3}	4.02^{-5}	1.65^{-6}	2.17^{-7}	2.59^{-8}	1.85^{-9}
	17	1.51^{-3}	1.78^{-3}	1.10^{-3}	1.35^{-3}	4.28^{-5}	1.76^{-6}	2.31^{-7}	2.75^{-8}	1.96^{-9}
	18	1.51^{-3}	1.80^{-3}	1.11^{-3}	1.37^{-3}	4.31^{-5}	1.77^{-6}	2.32^{-7}	2.77^{-8}	1.98^{-9}
	19	1.51^{-3}	1.80^{-3}	1.11^{-3}	1.37^{-3}	4.32^{-5}	1.77^{-6}	2.32^{-7}	2.78^{-8}	1.98^{-9}
T_e = 64000 °K	5	6.15^{-3}	1.77^{-3}	6.13^{-11}	1.37^{-13}	4.58^{-14}	1.82^{-14}	1.38^{-14}	1.16^{-14}	1.04^{-14}
	6	6.15^{-3}	1.77^{-3}	6.13^{-10}	1.37^{-12}	4.58^{-13}	1.81^{-13}	1.38^{-13}	1.16^{-13}	1.03^{-13}
	7	6.15^{-3}	1.77^{-3}	6.13^{-9}	1.37^{-11}	4.57^{-12}	1.81^{-12}	1.37^{-12}	1.15^{-12}	8.79^{-13}
	8	6.15^{-3}	1.77^{-3}	6.12^{-8}	1.37^{-10}	4.56^{-11}	1.79^{-11}	1.34^{-11}	1.08^{-11}	4.44^{-12}
	9	6.14^{-3}	1.76^{-3}	6.11^{-7}	1.37^{-9}	4.54^{-10}	1.75^{-10}	1.26^{-10}	7.26^{-11}	1.29^{-11}
	10	6.09^{-3}	1.75^{-3}	6.05^{-6}	1.36^{-8}	4.58^{-9}	1.60^{-9}	9.12^{-10}	2.54^{-10}	2.75^{-11}
	11	5.76^{-3}	1.69^{-3}	5.66^{-5}	1.34^{-7}	5.28^{-8}	1.31^{-8}	3.66^{-9}	6.27^{-10}	5.42^{-11}
	12	3.97^{-3}	1.34^{-3}	3.48^{-4}	1.21^{-6}	9.26^{-7}	7.95^{-8}	1.33^{-8}	1.79^{-9}	1.37^{-10}
	13	1.59^{-3}	8.63^{-4}	6.58^{-4}	9.98^{-6}	8.28^{-6}	3.99^{-7}	5.50^{-8}	6.77^{-9}	4.92^{-10}
	14	1.04^{-3}	7.97^{-4}	6.63^{-4}	8.53^{-5}	1.72^{-5}	7.53^{-7}	1.01^{-7}	1.22^{-8}	8.78^{-10}
	15	1.06^{-3}	1.11^{-3}	7.26^{-4}	5.22^{-4}	2.54^{-5}	1.08^{-6}	1.44^{-7}	1.74^{-8}	1.25^{-9}
	16	1.17^{-3}	1.53^{-3}	8.19^{-4}	1.09^{-3}	3.42^{-5}	1.45^{-6}	1.92^{-7}	2.31^{-8}	1.66^{-9}
	17	1.20^{-3}	1.63^{-3}	8.40^{-4}	1.22^{-3}	3.63^{-5}	1.53^{-6}	2.03^{-7}	2.44^{-8}	1.75^{-9}
	18	1.20^{-3}	1.64^{-3}	8.43^{-4}	1.24^{-3}	3.65^{-5}	1.54^{-6}	2.04^{-7}	2.45^{-8}	1.76^{-9}
	19	1.20^{-3}	1.64^{-3}	8.43^{-4}	1.24^{-3}	3.65^{-5}	1.54^{-6}	2.04^{-7}	2.45^{-8}	1.76^{-9}
T_e = 128000 °K	5	4.47^{-3}	1.27^{-3}	4.51^{-11}	1.38^{-13}	5.63^{-14}	2.45^{-14}	1.91^{-14}	1.61^{-14}	1.42^{-14}
	6	4.47^{-3}	1.27^{-3}	4.51^{-10}	1.38^{-12}	5.63^{-13}	2.45^{-13}	1.91^{-13}	1.61^{-13}	1.40^{-13}
	7	4.47^{-3}	1.27^{-3}	4.51^{-9}	1.38^{-11}	5.63^{-12}	2.44^{-12}	1.90^{-12}	1.59^{-12}	1.24^{-12}
	8	4.46^{-3}	1.27^{-3}	4.50^{-8}	1.37^{-10}	5.61^{-11}	2.42^{-11}	1.87^{-11}	1.51^{-11}	6.68^{-12}
	9	4.45^{-3}	1.27^{-3}	4.48^{-7}	1.37^{-9}	5.58^{-10}	2.37^{-10}	1.76^{-10}	1.07^{-10}	2.03^{-11}
	10	4.39^{-3}	1.26^{-3}	4.42^{-6}	1.37^{-8}	5.56^{-9}	2.23^{-9}	1.32^{-9}	3.95^{-10}	4.43^{-11}
	11	4.07^{-3}	1.21^{-3}	4.05^{-5}	1.35^{-7}	6.01^{-8}	1.76^{-8}	5.39^{-9}	9.67^{-10}	8.58^{-11}
	12	2.57^{-3}	9.89^{-4}	2.26^{-4}	1.27^{-6}	8.41^{-7}	9.25^{-8}	1.66^{-8}	2.34^{-9}	1.84^{-10}
	13	9.42^{-4}	7.50^{-4}	3.74^{-4}	1.15^{-5}	6.27	3.53^{-7}	5.11^{-8}	6.50^{-9}	4.84^{-10}
	14	6.14^{-4}	7.59^{-4}	3.61^{-4}	1.02^{-4}	1.28	6.28^{-7}	8.74^{-8}	1.09^{-8}	7.99^{-10}
	15	6.34^{-4}	1.11^{-3}	3.98^{-4}	5.83^{-4}	2.07^{-5}	9.65^{-7}	1.33^{-7}	1.63^{-8}	1.20^{-9}
	16	6.95^{-4}	1.50^{-3}	4.46^{-4}	1.12^{-3}	2.85^{-5}	1.30^{-6}	1.77^{-7}	2.18^{-8}	1.59^{-9}
	17	7.08^{-4}	1.58^{-3}	4.56^{-4}	1.23^{-3}	3.01^{-5}	1.37^{-6}	1.86^{-7}	2.29^{-8}	1.67^{-9}
	18	7.09^{-4}	1.59^{-3}	4.57^{-4}	1.24^{-3}	3.03^{-5}	1.37^{-6}	1.87^{-7}	2.30^{-8}	1.68^{-9}
	19	7.09^{-4}	1.59^{-3}	4.57^{-4}	1.24^{-3}	3.03^{-5}	1.38^{-6}	1.88^{-7}	2.30^{-8}	1.68^{-9}

Read : $6.74^{-3} = 6.74 \times 10^{-3}$

Table 6. Collisional-radiative ionization coefficients S_{C-R} ($cm^3\ sec^{-1}$) for an optically thin helium plasma.

T_e (°K)	8000	16000	32000	50000	64000	128000
log n_e						
5	1.54^{-24}	9.84^{-17}	1.07^{-12}	3.41^{-11}	1.36^{-10}	1.84^{-9}
6	1.55^{-24}	9.84^{-17}	1.07^{-12}	3.41^{-11}	1.36^{-10}	1.84^{-9}
7	1.55^{-24}	9.85^{-17}	1.07^{-12}	3.42^{-11}	1.36^{-10}	1.84^{-9}
8	1.55^{-24}	9.87^{-17}	1.07^{-12}	3.42^{-11}	1.37^{-10}	1.84^{-9}
9	1.56^{-24}	9.92^{-17}	1.08^{-12}	3.43^{-11}	1.37^{-10}	1.85^{-9}
10	1.58^{-24}	1.00^{-16}	1.08^{-12}	3.46^{-11}	1.38^{-10}	1.85^{-9}
11	1.63^{-24}	1.03^{-16}	1.11^{-12}	3.50^{-11}	1.39^{-10}	1.87^{-9}
12	1.93^{-24}	1.18^{-16}	1.21^{-12}	3.69^{-11}	1.44^{-10}	1.89^{-9}
13	5.90^{-24}	2.57^{-16}	1.86^{-12}	4.74^{-11}	1.73^{-10}	2.04^{-9}
14	2.74^{-23}	5.95^{-16}	2.75^{-12}	6.02^{-11}	2.08^{-10}	2.27^{-9}
15	7.06^{-23}	9.98^{-16}	3.62^{-12}	7.40^{-11}	2.51^{-10}	2.63^{-9}
16	2.94^{-22}	1.99^{-15}	4.87^{-12}	9.08^{-11}	2.99^{-10}	3.01^{-9}
17	7.34^{-22}	2.50^{-15}	5.24^{-12}	9.50^{-11}	3.10^{-10}	3.09^{-9}
18	8.78^{-22}	2.58^{-15}	5.29^{-12}	9.55^{-11}	3.11^{-10}	3.10^{-9}
19	8.95^{-22}	2.58^{-15}	5.29^{-12}	9.55^{-11}	3.12^{-10}	3.10^{-9}

Read : $1.54^{-24} = 1.54 \times 10^{-24}$

Table 7. Collisional-radiative recombination coefficients α_{C-R} ($cm^3\ sec^{-3}$) for an optically thin helium plasma.

T_e (°K)	8000	16000	32000	50000	64000	128000
log n_e						
5	4.43^{-13}	2.92^{-13}	1.89^{-13}	1.42^{-13}	1.21^{-13}	7.80^{-14}
6	4.45^{-13}	2.93^{-13}	1.89^{-13}	1.42^{-13}	1.21^{-13}	7.80^{-14}
7	4.56^{-13}	2.96^{-13}	1.90^{-13}	1.42^{-13}	1.21^{-13}	7.81^{-14}
8	4.86^{-13}	3.05^{-13}	1.93^{-13}	1.43^{-13}	1.22^{-13}	7.83^{-14}
9	5.47^{-13}	3.24^{-13}	1.99^{-13}	1.46^{-13}	1.23^{-13}	7.88^{-14}
10	6.61^{-13}	3.58^{-13}	2.09^{-13}	1.51^{-13}	1.27^{-13}	7.97^{-14}
11	8.73^{-13}	4.15^{-13}	2.26^{-13}	1.58^{-13}	1.31^{-13}	8.12^{-14}
12	1.30^{-12}	5.15^{-13}	2.51^{-13}	1.69^{-13}	1.38^{-13}	8.36^{-14}
13	2.23^{-12}	6.80^{-13}	2.77^{-13}	1.76^{-13}	1.41^{-13}	8.37^{-14}
14	4.44^{-12}	9.07^{-13}	2.99^{-13}	1.80^{-13}	1.42^{-13}	8.25^{-14}
15	8.92^{-12}	1.41^{-12}	3.77^{-13}	2.07^{-13}	1.58^{-13}	8.56^{-14}
16	3.41^{-11}	2.92^{-12}	5.17^{-13}	2.47^{-13}	1.79^{-13}	8.98^{-14}
17	1.12^{-10}	4.33^{-12}	6.21^{-13}	2.80^{-13}	1.99^{-13}	9.65^{-14}
18	4.73^{-10}	1.09^{-11}	1.26^{-12}	5.20^{-13}	3.54^{-13}	1.55^{-13}
19	3.94^{-9}	7.59^{-11}	7.63^{-12}	2.90^{-12}	1.90^{-12}	7.40^{-13}

Read : $4.43^{-13} = 4.43 \times 10^{-13}$

References

1) W.T. Silfvast; Appl. Phys. Letters, **13**, 169 (1968)
2) T.G. Giallorenzi and S.A. Ahmed; IEEE J. Quant. Electr., **QE-7**, 11 (1971)
3) G.J. Collins, R.C. Jensen and W.R. Bennett Jr.; Appl. Phys. Letters, **18**, 282 (1971)
4) R. Mewe; Physica, **47**, 373 (1970)
5) R. Mewe; Physica, **47**, 398 (1970)
6) N.P. Romanov; Opt. Spectr., **24**, 468 (1968)
7) Yu. A. Tolmachev; Opt. Spectr., **25**, 262 (1968)
8) D.R. Bates, A.E. Kingston and R.W.P. McWhirter; Proc. Roy. Soc., **A267**, 297 (1962)
9) R.W.P. McWhirter and A.G. Hearn; Proc. Fhys. Soc. **82**, 641 (1963)
10) T. Fujimoto, Y. Ogata, I. Sugiyama, K. Tachibana and K. Fukuda; Japanese J. Appl. Phys., **11**, 718 (1972)
11) H.W. Drawin and F. Emard; Zeit. Physik, **243**, 326 (1971)
12) H.W. Drawin and F. Emard; Rep. EUR-CEA-FC-534 Association Euratom-C.E.A. (1970)
13) H.W. Drawin, F. Klan and H. Ringler; Zeit. Naturforsch., **26a**, 186 (1971)
14) L. Tonks and I. Langmuir; Phys. Rev., **34**, 876 (1929)
15) W. Schottky; Phys. Zeit., **25**, 635 (1924)
16) E. Spenke; Zeit. Physik, **127**, 221 (1950)
17) J.H. Ingold; Zeit. Physik, **233**, 89 (1970)
18) T. Fujimoto, I. Sugiyama and K. Fukuda; THIS MEMOIRS, **34**, 249 (1972)
19) W.L. Wiese, M.W. Smith and B.M. Glennon; "Atomic Transition Probabilities -Hydrogen Through Neon NSRDS-NBS4," U.S. Department of Commerce (1966)
20) D.H. Menzel and C.L. Pekeris; Month. Not. Roy. Astr. Soc. (London), **96**, 77 (1935)
21) H.W. Drawin; Rep. EUR-CEA-FC-383 (revised) Association Euratom-C.E.A. (1967)
22) V.I. Ochkur and V.F. Bratsev; Opt. Spectr., **19**, 274 (1965)
23) I.P. Zapescohnyi; Soviet Astron., **AJ10**, 766 (1967)
24) L. Vriens and J.D. Carriere; Physica, **49**, 517 (1970)
25) K.L. Bell, D.J. Kennedy and A.E. Kingston; J. Phys., **B2**, 26 (1969)
26) P.G. Burke, J.W. Cooper and S. Ormonde; Phys. Rev., **183**, 245 (1969)
27) J.D. Jobe and R.M. St. John; Phys. Rev., **164**, 117 (1967)
28) V.I. Ochkur and V.F. Bratsev; Soviet Astron., **AJ9**, 797 (1966)
29) J. van Eck and J.P. De Jongh; Physica, **47**, 141 (1970)
30) L. Vriens, J.A. Simpson and S.R. Mielczarek; Phys. Rev., **165**, 7 (1968)
31) B.L. Moiseiwitsch; Month. Not. Roy. Astr. Soc. (London), **117**, 189 (1957)
32) R.E. Fox; J. Chem. Phys. **35**, 1379 (1961)
33) D. Rapp and P. Englander-Golden; J. Chem. Phys., **43**, 1464 (1965)
34) W. Lotz; Zeit. Physik, **232**, 101 (1970)
35) D.R. Long and R. Gevalle; Phys. Rev., **A1**, 260 (1970)
36) A. Dalgarno; Phil. Trans., **250**, 426 (1958)
37) A.V. Phelps; Phys. Rev., **99**, 1307 (1955)
38) T. Holstein; Phys. Rev., **72**, 1212 (1947)
39) T. Holstein; Phys. Rev., **83**, 1159 (1951)